

## A New hybrid radiotherapy technique for non-small cell lung cancer: Is more effective for functional lung sparing

C. Chen<sup>#</sup>, G. Chen<sup>#</sup>, R. Fang, Y. Xu, H. Liu\*, Z. Liao\*

Department of Radiation and Medical Oncology, Zhongnan Hospital of Wuhan University, Hubei Key Laboratory of Tumor Biological Behaviors, Hubei Cancer Clinical Study Center, Wuhan, 430071, Hubei, China

### ► Original article

**\*Corresponding author:**

Zhengkai Liao, MD, Ph.D.,

Hui Liu, MSc,

E-mail: zliao@whu.edu.cn,

liuhui69@hotmail.com

Received: July 2023

Final revised: January 2024

Accepted: February 2024

*Int. J. Radiat. Res.*, July 2024;  
22(3): 609-616

DOI: 10.61186/ijrr.22.3.609

**Keywords:** non-small-cell lung carcinoma, three dimensional conformal radiotherapy, intensity-modulated radiotherapy, respiratory function tests.

# These authors contributed equally to the work.

### INTRODUCTION

Radiotherapy is required in over 60% of lung cancer patients. When the cancer cannot be removed due to its size or location, if the patient is not healthy enough for surgery, or if the patient does not want surgery, an adequate radiation dose is an essential element for the successful treatment of patients with non-small cell lung cancer (NSCLC). However, radiation-induced lung toxicity (RILT) is a dose-limiting complication of traditional lung-directed radiotherapy. RILT includes radiation pneumonitis and pulmonary fibrosis, which can lead to deterioration of lung function, followed by lung failure and death<sup>(1,2)</sup>.

The conventional radiotherapy schedule for NSCLC is based on minimizing the radiation dose to the entire lung, regardless of the lung function. However, numerous studies have found regional differences in lung function<sup>(3,4)</sup>. The physical dose distribution and biological impact of the radiotherapy on functional lung need to be considered and optimized. The radiotherapy plan, which is called conventional functional intensity-modulated radiotherapy (IMRT), should be able to take

### ABSTRACT

**Background:** The Conventional thoracic radiotherapy planning ignores regional pulmonary function changes. This study aimed to evaluate the beneficial effect of a new hybrid three-dimensional conformal radiation therapy (3DCRT)/intensity-modulated radiation therapy (IMRT) technique. **Materials and Methods:** Thirty patients with non-small cell lung cancer were included in this study. Four protocols were designed for each patient: anatomical IMRT (A-IMRT, based on the total lung), functional IMRT (F-IMRT), pure IMRT (O-IMRT) plan, and hybrid 3DCRT/IMRT plan (H-3DCRT/IMRT), which were based on the functional lung. The opposing pair of fields in the O-IMRT and H-3DCRT/IMRT protocols provide 2/9 and 1/2 of radiation dose, respectively. The planning target volume coverage, dose in both total and functional lungs, maximum spinal cord dose, mean esophagus dose, mean heart dose, homogeneity index (HI), conformity index (CI), and treatment monitor units (MUs) were compared in this study. **Results:** The  $V_{5}$ ,  $V_{20}$ , and mean dose (Dmean) of the both total and functional lungs in the H-3DCRT/IMRT protocol were the lowest among the four treatment regimes. For D<sub>2</sub>, D<sub>98</sub>, HI, and CI, the A-IMRT protocol was superior to the H-3DCRT/IMRT protocol. Compared with the A-IMRT protocol, the F-IMRT protocol achieved significantly lower  $V_{5}$ ,  $V_{20}$ , and Dmean for functional lungs, but showed worse HI, CI, and maximum dose of spinal cord. The H-3DCRT/IMAT protocol significantly reduced the maximum spinal cord dose and MUs. **Conclusions:** The H-3DCRT/IMAT plan based on functional lung images appeared to be better than conventional F-IMRT in preserving functional lung without compromising on HI and CI in NSCLC patients.

advantage of regional differences within the lung, to deposit a lower radiation dose in the functional lung by adjusting the angle of the radiation field<sup>(5,6)</sup>.

Radiation-induced lung injury is more likely to occur in patients with poor lung function<sup>(7,8)</sup>, thus more protection should be given to patients with poor lung function. IMRT significantly improves dose conformity and reduces the dose to organs at risk (OARs), compared to three-dimensional conformal radiotherapy (3DCRT)<sup>(9)</sup>. Compared with IMRT, volumetric modulated arc therapy (VMAT) reduced irradiation time and treatment monitor units (MUs), improved target coverage, and decreased the dose to OARs<sup>(10-12)</sup>, but it increased the  $V_{5}$  and  $V_{10}$ <sup>(13)</sup>. The dose volume histogram parameters of  $V_{5}$  and  $V_{10}$  have been shown to predict radiation pneumonitis<sup>(14,15)</sup>, thus the VMAT technique may increase the incidence of radiation-induced pneumonitis (RIP). The IMRT plan is preferred for patients with poor lung function<sup>(16)</sup>.

In the IMRT plan, the modulated fields are designed to precisely deliver the dose to the targets. However, due to the seesaw effect, there are more limitations to sparing OARs, including functional lung, which are the worse results for modulating the

radiation beams to target volume and cancer control (17). This study examines the protection of functional lungs using a combination of 3DCRT and IMRT irradiation techniques. Compared to the currently used Functional IMRT (F-IMRT), the hybrid irradiation technique combines the advantages of both methods, specifically by reducing the radiation dose to both high functioning lungs and the entire lung through the use of a dual penetrating field technique and a 3DCRT technique. This approach effectively minimizes the occurrence of RLIT in patients with compromised lung function. Additionally, the hybrid technique ensures a balanced and optimal distribution of the target dose, taking into account both uniformity and conformity, through the use of the IMRT technique.

## MATERIALS AND METHODS

### Patients

Patients with poor lung function are more likely to have serious RLIT (18,19). Therefore, in this study we focused on NSCLC patients with poor lung function. This retrospective study included 30 patients (table 1) who underwent four-dimensional computed tomography (4DCT) scanning and definitive radiotherapy at Zhongnan Hospital of Wuhan University (Wuhan, China) from February 2019 to August 2019. These patients had abnormal baseline lung function forced vital capacity (FVC) of  $2.17 \pm 0.46$  L, forced expiration flow in 1 second (FEV<sub>1</sub>) of  $56.45 \pm 22.49\%$  and FEV<sub>1</sub>/FVC ratio of  $59.01 \pm 9.85\%$ . This study was based on routine examinations and treatments and was approved by the Independent Ethics Committee of Zhongnan Hospital of Wuhan University (approval number, 2023018K).

**Table 1.** Patient demographic information.

Category	Value	Percentage (%)
Sex		
Male	15	50
Female	15	50
Age		
Median	57	
Range	30-75	
Pathology		
Adenocarcinoma	14	47
Squamous cell carcinoma	16	53
Staging		
I	5	17
II	16	53
III	9	30

### Acquisition of functional lung images from 4DCT imaging

The ventilation imaging using 4DCT was developed for radiation treatment planning to identify the functional lung in patients with NSCLC (20,21). For each patient, a 4DCT scan was acquired with 2.0-mm-thick slices. A motion-monitoring

system delivering a motion surrogate signal was interfaced with a Siemens Somatom Sensation Open CT Scanner (120 kVp, 120 mA; Siemens Medical Systems AG, Erlangen, Germany) in cine mode using a Varian Real-time Position Management respiratory-gating system (Varian Medical Systems Inc., Palo Alto, CA, USA). We used the peak-inhale CT image as the reference image and the peak-exhale CT image as the floating image. The deformation vector field of different voxels in different respiratory phases was obtained using a cubic B-spline deformable image registration method. The accuracy of the B-spline registration method used has been thoroughly evaluated and the registration method is considered to meet the requirements of registration accuracy (22,23). The deformation vector field is converted to the Jacobian matrix using equation 1 (24,25). The Jacobian matrix represents the expansion or contraction of the local voxel when the image is transformed into another image, where the Jacobian value  $> 1$ , indicates the voxel expansion after deformation; the Jacobian value  $< 1$  represents voxel contraction after deformation; the Jacobian value = 1, represents no voxel change.

$$J(x, y, z) = \begin{vmatrix} 1 + \frac{\partial u_x(x, y, z)}{\partial x} & \frac{\partial u_x(x, y, z)}{\partial y} & \frac{\partial u_x(x, y, z)}{\partial z} \\ \frac{\partial u_y(x, y, z)}{\partial x} & 1 + \frac{\partial u_y(x, y, z)}{\partial y} & \frac{\partial u_y(x, y, z)}{\partial z} \\ \frac{\partial u_z(x, y, z)}{\partial x} & \frac{\partial u_z(x, y, z)}{\partial y} & 1 + \frac{\partial u_z(x, y, z)}{\partial z} \end{vmatrix} \quad (1)$$

$u$  is the deformation vector of the point  $(x, y, z)$  on the floating image relative to the reference image;  $u_x(x, y, z)$ ,  $u_y(x, y, z)$ ,  $u_z(x, y, z)$  are the components of  $u(x, y, z)$  in the  $x$ ,  $y$ ,  $z$  directions, respectively.

In equation (1),  $u$  is the deformation vector of the point  $(x, y, z)$  on the floating image relative to the reference image;  $u_x(x, y, z)$ ,  $u_y(x, y, z)$ ,  $u_z(x, y, z)$  are the components of  $u(x, y, z)$  in the  $x$ ,  $y$ ,  $z$  directions, respectively. Equation 1 is independently applied to each point of the lung in the floating image. At each point, the results are displayed in a pseudo-color map to obtain a lung ventilation image (figure 1). We define a region with a Jacobian value greater than 1.15 as a functional lung region (26).

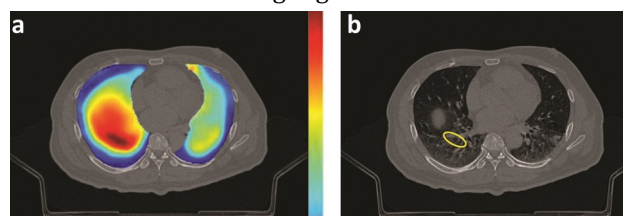


**Figure 1.** Example of lung ventilation image from a representative patient. The Ventilation imaging using 4DCT was developed to identify the functional lung. (a) A pseudo-color map displays the volume expansion of the lung. The more intense the red, the stronger the ventilation function; the more intense the blue, the weaker the ventilation function. (b) A region with a Jacobian value greater than 1.15 was defined as functional lung region, the area encircled by the yellow line.

### Planning using functional lung images

All dose calculations were performed using the peak-exhale CT images. The gross tumor volume (GTV) included both the primary tumor and metastatic lymph nodes, and a clinical target volume (CTV) margin of 8 mm was added to the GTV. Involved-field nodal irradiation was performed. Also, a planning target volume (PTV) margin of 8 mm was added allowing for reproducibility of respiratory motion and setup error for GTV and CTV. A total dose of 66 Gy in 33 fractions to 95% of the PTV was prescribed (27). Treatment plans were designed for a Varian Clinac iX Linear accelerator (Varian Medical Systems Inc.) using a 6 MV photon beam in the Eclipse® treatment planning system (version 13.5; Varian Medical systems Inc.).

For each patient, four radiotherapy plans (table 2) were designed and compared as shown below:

1. Anatomical IMRT (A-IMRT): A conventional anatomical IMRT plan based on the total lung. A 7-field dynamic multileaf collimator (DMLC) IMRT was used, and the illumination angle varied with the size, shape and position of the target area. The collimator angle was 0°.
2. Functional IMRT (F-IMRT): A conventional functional IMRT plan based on the functional lung. 7-field DMLC IMRT was used to reduce the absorbed dose in the functional lung by adjusting the angle of IMRT fields to avoid the functional lung volume.
3. Pure IMRT (O-IMRT): A 9-field DMLC IMRT plan was designed based on the A-IMRT with a pair of penetrating fields added. The beam angles of the penetrating fields were adjusted to avoid the high-function lung and the total lung to the largest extent. Since each field of the O-IMRT plan delivers the same dose, this pair of penetrating fields were planned to deliver 2/9 (22.2%) of the dose of 2 Gy (0.44 Gy).
4. Hybrid 3DCRT/IMRT (H-3DCRT/IMRT): According to functional lung, a hybrid 3DCRT/IMRT plan combined the 3DCRT and IMRT techniques. First, a two-field 3DCRT plan is generated, whose beam angles are the same as those of the two opposed fields of the O-IMRT plan. Then, based on this 3DCRT plan, a 7-field DMLC IMRT plan is generated, whose beam angles was from the A-IMRT plan. A 1/2 (50%) dose (1 Gy) was delivered by the 3DCRT and IMRT separately.

All plans had the same dose constraint, requiring a prescription dose curve covering 95% of the PTV volume, and the maximum dose of PTV not to exceed 110% of the prescribed dose. The dose to the OARs under the defined constraints is shown in table 3 (28). The calculation model used in this study was the Anisotropic Analytic Algorithm (AAA) with a 2 mm calculation grid size.

**Table 2.** The beam angles of the fields of the four radiotherapy plans used for a typical patient in this study.

	Beam Angles										
	A-IMRT	F-IMRT	O-IMRT	H-3DCRT/IMRT	210°	330°	350°	10°	140°	160°	180°
			195°	195°	210°	330°	350°	10°	140°	160°	180°
			15°	*15°	210°	330°	350°	10°	140°	160°	180°

\* Fields in the 3DRT planning (others were fields in the IMRT planning)  
IMRT: Intensity-modulated radiation therapy; 3DCRT: three-dimensional conformal radiation therapy; A-IMRT: anatomical IMRT based on the total lung; F-IMRT: functional IMRT based on the functional lung; O-IMRT: pure IMRT plan based on the functional lung; H-3DCRT/IMRT: hybrid 3DCRT/IMRT plan based on the functional lung.

**Table 3.** Dose limitation for organs at risk (OARs).

Vital organ	constraint
<b>Whole lung</b>	$V_5 < 65\%$
	$V_{20} < 37\%$
	Average dose < 20 Gy
<b>Functional lung</b>	$V_5 < 60\%$
	$V_{20} < 30\%$
	Average dose < 19 Gy
<b>Spinal cord</b>	Maximum dose < 47 Gy
<b>Esophagus</b>	Maximum dose < 70 Gy
	Average dose < 34 Gy
<b>Heart</b>	Maximum dose < 70 Gy
	$V_{60} < 33\%$
	$V_{45} < 66\%$

$V_5$ ,  $V_{20}$ ,  $V_{45}$ , and  $V_{60}$  ( $V_y$  = the percentage volume of the organ receiving a dose of  $y$  Gy or higher).

### Comparison and evaluation of plans

According to the International Commission on Radiation Units and Measurements report 83 (ICRU83 report) (29), the four plans were evaluated using the following terms:

1. Homogeneity Index (HI):  $HI = (D_2 - D_{98}) / D_{50}$ , a ratio evaluating the dose homogeneity in PTV.  $D_2$ ,  $D_{98}$ , and  $D_{50}$  are the minimum doses delivered to 2, 98, and 50% volume of the PTV, respectively. An HI of zero indicates that the absorbed-dose distribution is almost homogeneous.
2. Conformity Index (CI):  $CI = (V_{T,ref} \times V_{T,ref}) / (V_t \times V_{ref})$ , where  $V_t$  is the target volume and  $V_{ref}$  is the volume of all regions surrounded by the reference isodose line;  $V_{T,ref}$  is the volume of the target area surrounded by the reference isodose line; CI of 1 indicates that the prescribed dose volume is very consistent with the target area.
3. Target volumes:  $D_{98}$ ,  $D_{95}$ ,  $D_{50}$  and  $D_2$  were the minimum dose delivered to 98, 95, 50, and 2% volume of the PTV, respectively.
4. Normal structures:  $D_{max}$  is the maximum dose for spinal cord. Both total and functional lungs were analyzed with  $V_5$ ,  $V_{20}$ , and mean lung dose (MLD).  $V_5$  and  $V_{20}$  represent the volume of normal tissue receiving  $\geq 5$  Gy and  $\geq 20$  Gy, respectively. The heart and esophagus were analyzed using the mean dose.

5. Number of monitor units (MUs): The number of monitor units required to deliver the radiation dose was analyzed for all plans.

6. Planning time: The planning time for plans is dominated by performing optimization iterations with the system (*i.e.*, setting parameters, having the system perform the optimization, evaluating the results, and repeating until the planner is satisfied).

### Statistical analysis

The GraphPad Prism v5.0 software (GraphPad Software inc, San Diego, CA, USA) was used for all statistical analyses. For pairwise comparison of the groups, one-way analysis of variance (ANOVA) and paired sample *t* - test were used. Statistical significance was defined as  $p < 0.05$ .

## RESULTS

### Lung ventilation image

Representative ventilation and functional lung images obtained by 4DCT are shown in figure 1. In these pseudo color images, the more intense the red, the greater the Jacobian value, which means large volume expansion and high ventilation function. Conversely, the more intense the blue, the weaker the function. Functional lung region is encircled by a yellow line (figure 1b).

### Comparison of dosimetric parameters

As shown in table 2, different fields of the four radiotherapy plans were designed for each patient. All of which were IMRT fields except for two 3DRT fields in the H-3DCRT/IMRT plan, which were different from the O-IMRT plan. These plans meet the same dosimetric criteria.

Examples of typical dose distribution are shown in figure 2. The HI of the A-IMRT and O-IMRT plans were  $0.0408 \pm 0.0615$  and  $0.0401 \pm 0.0413$ , respectively, while the CI of the A-IMRT and O-IMRT plans were  $0.7664 \pm 0.0885$  and  $0.7670 \pm 0.0695$ , respectively. The H-3DCRT/IMRT plan ( $HI = 0.0569 \pm 0.0243$ ,  $CI = 0.7405 \pm 0.0785$ ) was in the middle, while the F-IMRT plan ( $HI = 0.0752 \pm 0.0378$ ,  $CI = 0.7139 \pm 0.0953$ ) was the worst. There was no significant difference between  $D_{50}$  and  $D_{95}$  among the four plans.

Since the cumulative dose volume histogram (DVH) can summarize the simulated radiation distribution within a volume of interest of a patient, the DVH was used to compare the dose in the PTV (figure 3a), total lung (figure 3b), and functional lung (figure 3c) for the four plans. As shown in figure 3 and table 4, for the protection of OARs, the H-3DCRT/IMRT plan most significantly decreased  $V_5$ ,  $V_{20}$ , and  $D_{mean}$  of both total and functional lungs. Compared

with the A-IMRT plan, the F-IMRT plan had lower  $V_5$ ,  $V_{20}$ , and  $D_{mean}$  of both total and functional lungs ( $p < 0.05$ ), while sacrificing both homogeneity and conformity ( $p = 0.0297$ ,  $p = 0.0357$ ), and increased the  $D_{max}$  of the spinal cord ( $p = 0.0133$ ). In addition, the data in table 4 show that planned MUs per fraction were significantly lower for the H-3DCRT/IMRT plan ( $834.67 \pm 70.47$ ) than for the A-IMRT ( $1189 \pm 68.74$ ), F-IMRT ( $1318.33 \pm 147.55$ ) and O-IMRT ( $1336.49 \pm 104.32$ ) plans ( $p < 0.05$ ). In terms of the planning time, the H-3DCRT/IMRT plan ( $1690.36s \pm 148.28s$ ), O-IMRT plan ( $1647.31s \pm 133.56s$ ), and A-IMRT plan ( $1621.25s \pm 155.27s$ ) were similar and shorter than the F-IMRT plan ( $1733.74 \pm 182.69$ ). There was no statistical difference in  $D_{mean}$  of esophagus and heart among these four plans.

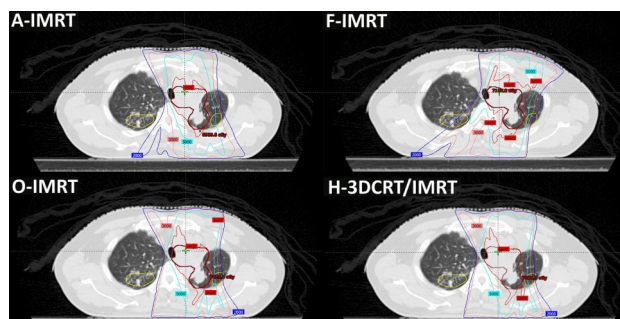


**Figure 2.** The isodose distribution of axial views generated from the four treatment plans (A-IMRT, F-IMRT, O-IMRT, and H-3DCRT/IMRT) in the same representative patient. V20: dark blue contour; V30: pink contour; V50: light blue contour; V66: light red contour; PTV: dark red contour; Functional lung: yellow contour.

A typical case is illustrated in Figure 4, showcasing the influence of gantry angles on irradiation in the A-IMRT plan. Notably, beams at  $140^\circ$  (field 3) and  $330^\circ$  (field 6) contribute significantly more to total functional lung irradiation (figure 4a). In response, the F-IMRT plan adjusted these angles, reducing absorbed radiation in functional lungs. Compared to the A-IMRT plan, the F-IMRT plan showed lower  $V_5$ ,  $V_{20}$ , and  $D_{mean}$  for functional lungs, but showed worse HI, CI, and  $D_{max}$  for spinal cord (table 4). In addition, since the  $160^\circ$  (field 2) and  $350^\circ$  (field 5) fields contributed 307.0 cGy and 320.7 cGy to the functional lung dose, respectively, adjusting these two field angles may further reduce the radiation dose in the functional lung. However, the  $D_{max}$  for the spinal cord was further increased after adjustment (figure 4b). While offering improved functional lung dose distribution, the O-IMRT limits protection due to the small contribution of its opposing fields. In addition, the O-IMRT plan yields a higher total lung dose compared to the A-IMRT plan.

**Table 4.** Comparison of dosimetric parameters of the A-IMRT, F-IMRT, O-IMRT, and H-3DCRT/IMRT plans.

		A-IMRT Mean (SD)	F-IMRT Mean (SD)	O-IMRT Mean (SD)	H-3DCRT/ IMRT Mean (SD)	ANOVA	Paired t-test				
							A-IMRT vs F-IMRT	A-IMRT vs O-IMRT	A-IMRT vs H-3DCRT/ IMRT	F-IMRT Vs H-3DCRT/ IMRT	O-IMRT Vs H-3DCRT/ IMRT
PTV	D2	6905.42 (36.16)	7049.77 (81.39)	7013.47 (53.82)	7025.92 (47.55)	0.026	0.0385	0.0459	0.0421	0.0496	0.6121
	D50	6716.67 (34.77)	6737.5 (79.08)	6729.56 (44.81)	6718.38 (47.35)	0.867	0.6615	0.6925	0.7411	0.6887	0.7052
	D98	6591.12 (33.98)	6525.53 (36.92)	6608.54 (38.24)	6578.87 (43.25)	0.0213	0.0341	0.0419	0.0484	0.0461	0.0554
	D95	6644.06 (26.56)	6626.84 (38.38)	6650.19 (41.36)	6639.56 (49.97)	0.6025	0.6265	0.7183	0.8257	0.6439	0.6935
	HI	0.0408 (0.0615)	0.0752 (0.0378)	0.0401 (0.0413)	0.0569 (0.0243)	0.0038	0.0197	0.0632	0.0538	0.0437	0.0529
	CI	0.7664 (0.0885)	0.7139 (0.0953)	0.7670 (0.0695)	0.7505 (0.0785)	0.0205	0.0257	0.0671	0.0571	0.0394	0.0666
Total Lung	V5	36.27 (14.33)	32.53 (13.61)	38.67 (17.26)	30.02 (12.75)	0.0196	0.0285	0.0434	0.0136	0.0486	0.0087
	V20	20.33 (11.27)	18.56 (11.11)	22.57 (14.38)	16.13 (10.74)	0.0252	0.0262	0.0317	0.0423	0.0384	0.0069
	Dmean	996.93 (28.98)	944.97 (31.55)	1034.78 (44.26)	885.93 (57.76)	0.017	0.0376	0.0401	0.0259	0.0371	0.0115
Functional Lung	V5	40.27 (13.91)	37.33 (15.56)	38.64 (12.64)	35.07 (14.02)	0.0082	0.0418	0.0486	0.0124	0.0313	0.0233
	V20	31.67 (14.83)	26.72 (13.81)	28.92 (15.21)	23.19 (13.17)	0.0211	0.0366	0.0455	0.0207	0.0434	0.0312
	Dmean	1301.77 (239.07)	1188.6 (183.34)	1242.84 (149.27)	975.5 (190.54)	0.0065	0.0321	0.0399	0.0077	0.0217	0.0164
Spinal Cord	Dmax	3524.63 (53.41)	3867.4 (83.8)	3540.82 (69.38)	3546.37 (99.97)	0.0257	0.0333	0.1282	0.0559	0.0385	0.1701
Esophagus	Dmean	3351.43 (137.76)	3344.77 (124.1)	3366.46 (147.38)	3392.97 (170.17)	0.6284	0.7221	0.5416	0.1727	0.1002	0.2263
Heart	Dmean	192.4 (10.25)	177.7 (12.63)	183.6 (27.31)	180.6 (22.94)	0.0752	0.0528	0.1615	0.1204	0.2598	0.1946
MUs		1189 (68.74)	1318.33 (147.55)	1336.49 (104.32)	834.67 (70.47)	0.0247	0.0427	0.0392	0.0296	0.0238	0.0131
Planning time		1621.25 (155.27)	1733.74 (182.69)	1647.31 (133.56)	1670.36 (148.28)	0.0454	0.0425	0.1013	0.0621	0.0487	0.0856

$D_{98}$ ,  $D_{95}$ ,  $D_{50}$ , and  $D_2$  (Dy = the minimum dose delivered to y % volume of the PTV); HI: homogeneity index; CI: conformity index; Dmean: the mean dose; Dmax: the maximum dose.

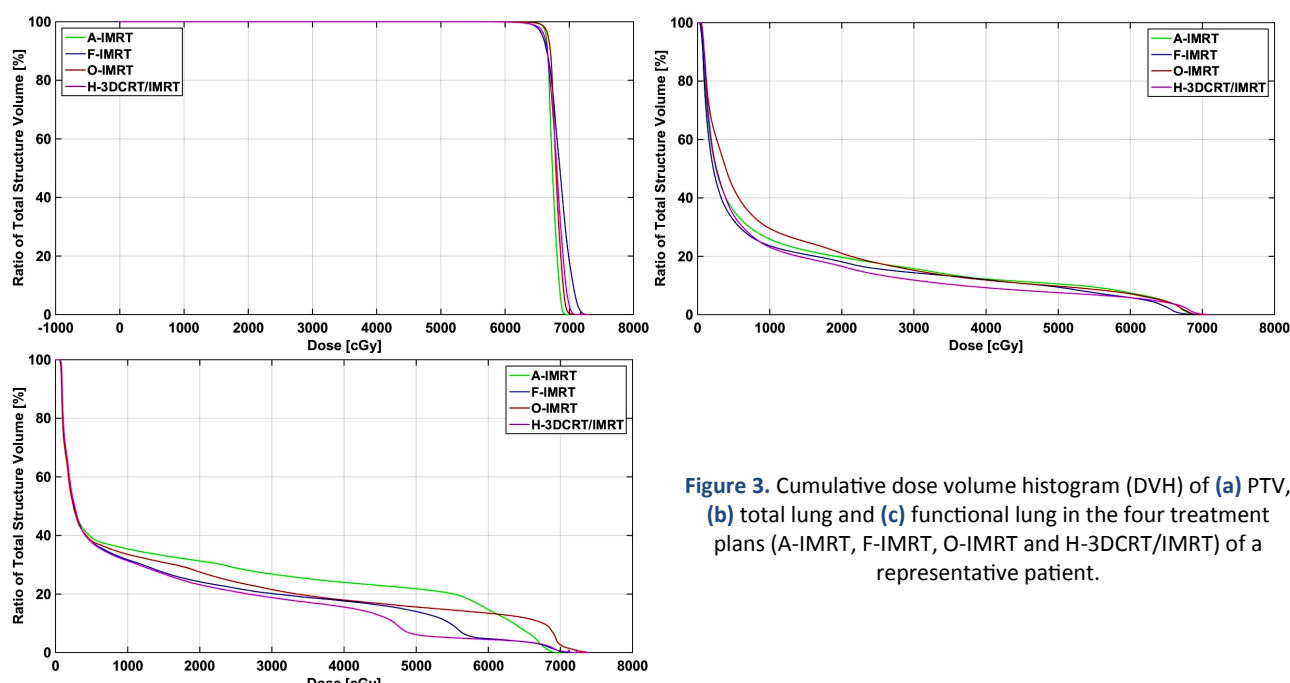


**Figure 3.** Cumulative dose volume histogram (DVH) of (a) PTV, (b) total lung and (c) functional lung in the four treatment plans (A-IMRT, F-IMRT, O-IMRT and H-3DCRT/IMRT) of a representative patient.

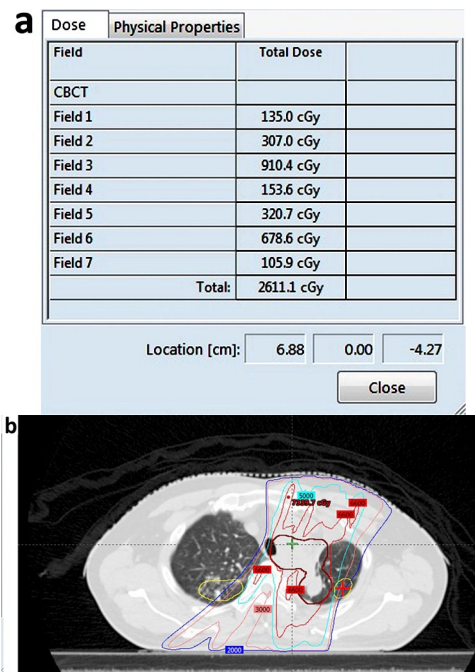


**Figure 4.** Example of a typical patient treated with radiotherapy illustrating the dose contribution of radiation fields. (a) Dose contribution from each field in the A-IMRT plan to a certain point (the red cross in the left lung in Figure 4b); (b) Dose distribution in the F-IMRT plan, which was from A-IMRT after adjusting Field 2 (160°), Field 3 (140°), Field 5 (350°) and Field 6 (330°) in Figure 4a to avoid functional lung.

## DISCUSSION

Thoracic radiotherapy remains one of the standard treatments for NSCLC. IMRT may be more suitable than 3DCRT for patients with poor lung function, as sparing the surrounding critical structures from toxicity was of particular concern<sup>(30)</sup>. Chang *et al.* found that advanced lung cancer has a large GTV and complicated position within normal tissue, so lung function is often poor, and IMRT was a better choice for the treatment than 3DCRT, as a result of a better dose distribution<sup>(31)</sup>.

Radiation-induced lung injury, including radiation pneumonitis and radiation fibrosis, was the most common treatment-limiting toxicity among patients who received thoracic radiotherapy. It is important to carefully consider dosimetric factors, especially in functional lung regions<sup>(32, 33)</sup>. Studies have shown that radiation-induced lung injury is closely related to the lung volume of low-dose irradiation<sup>(34)</sup>. V<sub>5</sub> and V<sub>20</sub> are dosimetric risk factors for the incidence and severity of RILT, and can be used as predictors of radiation pneumonia<sup>(35)</sup>. Since patients with advanced NSCLC had poor lung function and VMAT had larger volume of low-dose irradiation than IMRT<sup>(36)</sup>, IMRT was used in this study. However, IMRT planning minimizes the radiation dose to the anatomical lungs despite regional pulmonary function variations<sup>(37)</sup>.

Functional imaging was used to delineate the functional lung region for NSCLC functional radiotherapy planning, resulting in a significantly decreased dose to avoid well-functioning lung<sup>(38)</sup>. Functional measurements have been evaluated in NSCLC radiotherapy, including single photon emission computed tomography (SPECT), 4DCT and hyperpolarized noble gas magnetic resonance imaging (MRI)<sup>(39)</sup>. Ventilation imaging is one of the popular modalities, which was generated from components of the 4DCT sets using a deformable image registration algorithm<sup>(32)</sup>. Conventional functional IMRT adjusts the angles of the radiation fields to avoid functional lung regions<sup>(20,32)</sup>, but it always leads to a poor dose distribution, which may cause hot or cold spots in the target area and OAR.

Farr *et al.* reported using SPECT to guide treatment planning, and found that functional avoidance plans can reduce the irradiation of the functional lung in patients with locally advanced lung cancer<sup>(40)</sup>. They observed that IMRT better protects the functional lung compared to 3DCRT and VMAT. Mounessi *et al.* evaluated the feasibility of using the functional lung in the treatment of NSCLC, and showed that incorporating functional imaging into radiotherapy planning appears to be beneficial in preserving a functional lung in NSCLC<sup>(41)</sup>. They also found that functional IMRT results in lower functional lung doses compared to functional VMAT. Zhou *et al.* incorporated 4DCT ventilation function images into radiotherapy planning for esophageal cancer to evaluate the functional lung protection effects of different radiotherapy plans<sup>(42)</sup>. They found that conventional functional IMRT can reduce the dose to the functional lung and lung tissue but also decreases the CI of the PTV. In the case of protective plans for the functional lung, although 5F-IMRT (IMRT plan with 5 fields) reduces radiation doses to lung tissue and the heart, it lags behind 7F-IMRT and 9F-IMRT in terms of the PTV consistency.

Our results are consistent with the conclusions of the above-mentioned studies. To address the issue of decreased CI of the PTV in adaptive plans guided by functional imaging while protecting the functional lung, we propose the use of a hybrid radiotherapy approach. Hybrid radiotherapy is a combination of different techniques, which may combine their advantages. Different treatment planning can result in different dose distribution. Chan *et al.* used two static fields conformal radiotherapy combined with VMAT to obtain lower mean and maximum spinal cord dose and lower risk of complication of the lung<sup>(43)</sup>. Zhao *et al.* combined IMRT with VMAT to treat NSCLC and significantly reduced the lung radiation dose<sup>(44)</sup>. However, the hybrid technique has not been used in functional lung avoidance.

In this study, a hybrid 3DCRT/IMRT planning approach based on functional lung imaging was used, which compared with F-IMRT, it can greatly improve

the dosimetric parameters for total and functional lungs, while at the same time optimizing the dose distribution of target volumes and OARs. The reasons for these improvements were the opposed fields in 3DCRT of the hybrid planning covering the majority of PTV, while minimizing the dose of OARs including functional lung and total lung, and also that IMRT delivered the radiation dose precisely to the target volume.

Although the hybrid 3DCRT/IMRT and O-IMRT plans have the same beam angles of fields, the H-3DCRT/IMRT showed a lower dose of functional lungs, due to the increase of the dose weight of the penetrating fields from 22.2% (O-IMRT) to 50% (3DCRT/IMRT). In fact, if this dose weight was too high, the conformity of treatment plan would become worse, and if this dose weight was too low, it could not adequately protect the functional lungs. Thus, in order to balance their benefits and drawbacks, the median value of 50% was used in this study. We believe this is an important effort.

In addition, the H-3DCRT/IMRT plan did not significantly increase the planning time ( $p > 0.05$ ), due to the simple design of the penetrating fields. Furthermore, the H-3DCRT/IMRT plan significantly reduced treatment time and MUs, which was beneficial to both the patients and the machines. Wang et al. demonstrated that reducing the treatment time of a single fraction may improve the therapeutic effect (45). Less MUs reduces the incidence of secondary radiation-induced cancer (46), while improving the efficiency of the linear accelerator and reducing machine wear.

## CONCLUSION

The hybrid 3DCRT/IMRT planning is a promising technique, which resulted in further reductions of the radiation dose in functional and total lung compared with the conventional functional IMRT. The effect of different weights of the fields warrants further study. Since the 3DCRT, IMRT, and 4DCT techniques are widely used, this hybrid technique has a broad application prospect.

**Finding:** This research did not receive any specific grant from funding agencies in the public, commercial, or not-for-profit sectors.

**Conflict of interest:** The authors declare that the research was conducted in the absence of any commercial or financial relationships that could be construed as a potential conflict of interest.

**Ethics statement:** Approval was acquired from the clinical ethics committee of ZhongNan Hospital of Wuhan University (approval number, 2023018K).

**Author contributions:** C.C.: Conceptualization, Methodology, Data Curation, Formal analysis, Writing - Original Draft; G.C.: Conceptualization, Methodology,

Formal analysis, Writing-Original Draft; R.F.: Data Curation, Writing-Original Draft; Y.X.: Data Curation, Writing-Original Draft; H.L.: Conceptualization, Supervision, Writing-Review & Editing; Z.L.: Conceptualization, Project administration, Supervision, Writing-Review & Editing; All authors contributed to the article and approved the submitted version.

## REFERENCES

1. Jiang ZQ, Yang K, Komaki R, et al. (2012) Long-term clinical outcome of intensity-modulated radiotherapy for inoperable non-small cell lung cancer: the MD Anderson experience. *Int J Radiat Oncol Biol Phys*, **83**(1):332-339.
2. Mazeran R, Etienne-Mastroianni B, Perol D, et al. (2010) Predictive factors of late radiation fibrosis: a prospective study in non-small cell lung cancer. *Int J Radiat Oncol Biol Phys*, **77**(1):38-43.
3. Rankine LJ, Wang Z, Driehuys B, et al. (2018) Correlation of Regional Lung Ventilation and Gas Transfer to Red Blood Cells: Implications for Functional-Avoidance Radiation Therapy Planning. *Int J Radiat Oncol Biol Phys*, **101**(5):1113-1122.
4. Tahir BA, Hughes P, Robinson SD, et al. (2018) Spatial Comparison of CT-Based Surrogates of Lung Ventilation with Hyperpolarized Helium-3 and Xenon-129 Gas MRI in Patients Undergoing Radiation Therapy. *Int J Radiat Oncol Biol Phys*, **102**(4):1276-1286.
5. Bucknell NW, Hardcastle N, Bressel M, et al. (2018) Functional lung imaging in radiation therapy for lung cancer: A systematic review and meta-analysis. *Radiother Oncol*, **129**(2):196-208.
6. Hegi-Johnson F, de Ruyscher D, Keall P, et al. (2019) Imaging of regional ventilation: Is CT ventilation imaging the answer? A systematic review of the validation data. *Radiother Oncol*, **137**:175-185.
7. Hong A, Dische S, Saunders MI, et al. (1991) Lung function and radiation response. *Br J Radiol*, **64**(768):1134-1139.
8. Rubin P, Finkelstein J, Shapiro D (1992) Molecular biology mechanisms in the radiation induction of pulmonary injury syndromes: interrelationship between the alveolar macrophage and the septal fibroblast. *Int J Radiat Oncol Biol Phys*, **24**(1):93-101.
9. Murshed H, Liu HH, Liao Z, et al. (2004) Dose and volume reduction for normal lung using intensity-modulated radiotherapy for advanced-stage non-small-cell lung cancer. *Int J Radiat Oncol Biol Phys*, **58**(4):1258-1267.
10. McGrath SD, Matuszak MM, Yan D, et al. (2010) Volumetric modulated arc therapy for delivery of hypo fractionated stereotactic lung radiotherapy: A dosimetric and treatment efficiency analysis. *Radiother Oncol*, **95**(2):153-157.
11. Ong CL, Verbakel WF, Cuijpers JP, et al. (2010) Stereotactic radiotherapy for peripheral lung tumors: a comparison of volumetric modulated arc therapy with 3 other delivery techniques. *Radiother Oncol*, **97**(3):437-442.
12. Rao M, Yang W, Chen F, et al. (2010) Comparison of Elekta VMAT with helical tomotherapy and fixed field IMRT: plan quality, delivery efficiency and accuracy. *Med Phys*, **37**(3):1350-1359.
13. Jiang X, Li T, Liu Y, et al. (2011) Planning analysis for locally advanced lung cancer: dosimetric and efficiency comparisons between intensity-modulated radiotherapy (IMRT), single-arc/partial-arc volumetric modulated arc therapy (SA/PA-VMAT). *Radiation oncology (London, England)*, **6**(1):140.
14. Abbas AS, Moseley D, Kassam Z, et al. (2013) Volumetric-modulated arc therapy for the treatment of a large planning target volume in thoracic esophageal cancer. *J Appl Clin Med Phys*, **14**(3):4269.
15. Wang S, Liao Z, Wei X, et al. (2006) Analysis of clinical and dosimetric factors associated with treatment-related pneumonitis (TRP) in patients with non-small-cell lung cancer (NSCLC) treated with concurrent chemotherapy and three-dimensional conformal radiotherapy (3D-CRT). *Int J Radiat Oncol Biol Phys*, **66**(5):1399-1407.
16. Li Y, Wang J, Tan L, et al. (2018) Dosimetric comparison between IMRT and VMAT in irradiation for peripheral and central lung cancer. *Oncol Lett*, **15**(3):3735-3745.
17. Shiroyama Y, Jang SY, Liu HH, et al. (2007) Preserving functional lung using perfusion imaging and intensity-modulated radiation therapy for advanced-stage non-small cell lung cancer. *Int J Radiat Oncol*

*Biol Phys*,**68**(5):1349-1358.

18. Robnett TJ, Machtay M, Vines EF, et al. (2000) Factors predicting severe radiation pneumonitis in patients receiving definitive chemoradiation for lung cancer. *Int J Radiat Oncol Biol Phys*,**48**(1):89-94.
19. Lind PA, Marks LB, Hollis D, et al. (2002) Receiver operating characteristic curves to assess predictors of radiation-induced symptomatic lung injury. *Int J Radiat Oncol Biol Phys*,**54**(2):340-347.
20. Vinogradskiy Y, Castillo R, Castillo E, et al. (2022) Results of a Multi-Institutional Phase 2 Clinical Trial for 4DCT-Ventilation Functional Avoidance Thoracic Radiation Therapy. *Int J Radiat Oncol Biol Phys*,**112**(4):986-995.
21. Faught AM, Olsen L, Schubert L, et al. (2018) Functional-guided radiotherapy using knowledge-based planning. *Radiother Oncol*,**129**(3):494-498.
22. Yamamoto T, Kabus S, Klinder T, et al. (2011) Four-dimensional computed tomography pulmonary ventilation images vary with deformable image registration algorithms and metrics. *Med Phys*,**38**(3):1348-1358.
23. Kybic J and Unser M (2003) Fast parametric elastic image registration. *IEEE Trans Image Process*,**12**(11):1427-1442.
24. Cui T, Miller GW, Mugler JR, et al. (2018) An initial investigation of hyperpolarized gas tagging magnetic resonance imaging in evaluating deformable image registration-based lung ventilation. *Med Phys*,**45**(12):5535-5542.
25. Christensen GE, Song JH, Lu W, et al. (2007) Tracking lung tissue motion and expansion/compression with inverse consistent image registration and spirometry. *Med Phys*,**34**(6):2155-2163.
26. Reinhardt JM, Ding K, Cao K, et al. (2008) Registration-based estimates of local lung tissue expansion compared to xenon CT measures of specific ventilation. *Med Image Anal*,**12**(6):752-763.
27. Lei W, Jia J, Cao R, et al. (2017) Impacts of lung and tumor volumes on lung dosimetry for nonsmall cell lung cancer. *J Appl Clin Med Phys*,**18**(5):22-28.
28. Yamamoto T, Kabus S, Bal M, et al. (2016) The first patient treatment of computed tomography ventilation functional image-guided radiotherapy for lung cancer. *Radiother Oncol*,**118**(2):227-231.
29. Hodapp N (2012) [The ICRU Report 83: prescribing, recording and reporting photon-beam intensity-modulated radiation therapy (IMRT)]. *Strahlenther Onkol*,**188**(1):97-99.
30. Liu HH, Wang X, Dong L, et al. (2004) Feasibility of sparing lung and other thoracic structures with intensity-modulated radiotherapy for non-small-cell lung cancer. *Int J Radiat Oncol Biol Phys*,**58**(4):1268-1279.
31. Chang JY (2015) Intensity-modulated radiotherapy, not 3 dimensional conformal, is the preferred technique for treating locally advanced lung cancer. *Semin Radiat Oncol*,**25**(2):110-116.
32. O'Reilly S, Jain V, Huang Q, et al. (2020) Dose to Highly Functional Ventilation Zones Improves Prediction of Radiation Pneumonitis for Proton and Photon Lung Cancer Radiation Therapy. *Int J Radiat Oncol Biol Phys*,**107**(1):79-87.
33. Yamamoto T, Kabus S, Bal M, et al. (2018) Changes in Regional Ventilation During Treatment and Dosimetric Advantages of CT Ventilation Image Guided Radiation Therapy for Locally Advanced Lung Cancer. *Int J Radiat Oncol Biol Phys*,**102**(4):1366-1373.
34. Shi A, Zhu G, Wu H, et al. (2010) Analysis of clinical and dosimetric factors associated with severe acute radiation pneumonitis in patients with locally advanced non-small cell lung cancer treated with concurrent chemotherapy and intensity-modulated radiotherapy. *Radiat Oncol*,**5**:35.
35. Wang D, Shi J, Liang S, et al. (2013) Dose-volume histogram parameters for predicting radiation pneumonitis using receiver operating characteristic curve. *Clin Transl Oncol*,**15**(5):364-369.
36. Teoh M, Clark CH, Wood K, et al. (2011) Volumetric modulated arc therapy: a review of current literature and clinical use in practice. *Br J Radiol*,**84**(1007):967-996.
37. Sura S, Gupta V, Yorke E, et al. (2008) Intensity-modulated radiation therapy (IMRT) for inoperable non-small cell lung cancer: The Memorial Sloan-Kettering Cancer Center (MSKCC) experience. *Radiother Oncol*,**87**(1):17-23.
38. Faught AM, Miyasaka Y, Kadoya N, et al. (2017) Evaluating the Toxicity Reduction with Computed Tomographic Ventilation Functional Avoidance Radiation Therapy. *Int J Radiat Oncol Biol Phys*,**99**(2):325-333.
39. Hodge CW, Tome WA, Fain SB, et al. (2010) On the use of hyperpolarized helium MRI for conformal avoidance lung radiotherapy. *Med Dosim*,**35**(4):297-303.
40. Farr KP, West K, Yeghiaian-Alvandi R, et al. (2019) Functional perfusion image guided radiation treatment planning for locally advanced lung cancer. *Phys Imaging Radiat Oncol*,**11**:76-81.
41. Mounessi FS, Eckardt J, Holstein A, et al. (2020) Image-based lung functional radiotherapy planning for non-small cell lung cancer. *Strahlenther Onkol*,**196**(2):151-158.
42. Zhou PX, Wang RH, Yu H, et al. (2022) Different functional lung-sparing strategies and radiotherapy techniques for patients with esophageal cancer. *Front Oncol*,**12**:898141.
43. Chan OS, Lee MC, Hung AW, et al. (2011) The superiority of hybrid-volumetric arc therapy (VMAT) technique over double arcs VMAT and 3D-conformal technique in the treatment of locally advanced non-small cell lung cancer--a planning study. *Radiother Oncol*,**101**(2):298-302.
44. Zhao N, Yang R, Wang J, et al. (2015) An IMRT/VMAT Technique for Nonsmall Cell Lung Cancer. *Biomed Res Int*,**2015**:1-7.
45. Wang JZ, Li XA, D'Souza WD, Stewart RD (2003) Impact of prolonged fraction delivery times on tumor control: a note of caution for intensity-modulated radiation therapy (IMRT). *Int J Radiat Oncol Biol Phys*,**57**(2):543-552.
46. Hall EJ (2006) Intensity-modulated radiation therapy, protons, and the risk of second cancers. *Int J Radiat Oncol Biol Phys*,**65**(1):1-7.